

# A Color Mutation Model of Soft Interaction in High Energy Hadronic Collisions

Zhen Cao\* and Rudolph C. Hwa†

Institute of Theoretical Science and Department of Physics  
University of Oregon, Eugene, OR 97403-5203, USA

A comprehensive model, called ECOMB, is proposed to describe multiparticle production by soft interaction. It incorporates the eikonal formalism, parton model, color mutation, branching and recombination. The physics is conceptually opposite to the dynamics that underlies the fragmentation of a string. The partons are present initially in a hadronic collision; they form a single, large, color-neutral cluster until color mutation of the quarks leads to a fission of the cluster into two color-neutral subclusters. The mutation and branching processes continue until only  $q\bar{q}$  pairs are left in each small cluster. The model contains self-similar dynamics and exhibits scaling behavior in the factorial moments. It can satisfactorily reproduce the intermittency data that no other model has been able to fit.

## I. INTRODUCTION

The study of multiparticle production in low- $p_T$  processes has been pursued for over twenty years. Since they involve soft interactions, they cannot be treated in perturbative QCD. In the absence of any reliable theoretical approach to the problem, many models have been proposed, most of which are represented in the review volumes published ten years ago [1,2]. Nearly all of those models have since been shown to be inadequate in light of the data on fluctuations and intermittency [3,4]. Indeed, there are very few models that have the appropriate dynamical content capable of reproducing the scaling behaviors observed in the experiments. Even though perturbative QCD cannot be used, it seems that some kind of branching process is needed to generate the property of self-similarity, as the resolution scale is varied. In this paper we propose a model that incorporates some aspects of nonperturbative QCD and is capable of generating the features of the intermittency data, which are shown in the last figure of this paper. To our knowledge those data have not been fitted by any model that contains some features of the color dynamics. To reproduce those data has become the main motivator for this work.

Our approach embraces many time-honored properties of hadronic collisions. Since hadrons are extended objects, the eikonal formalism is at the foundation of our model. Thus it is not difficult for our model to possess the virtues of geometrical scaling [5] and approximate KNO scaling [6]. In order to build into the model features of chromodynamics, it is necessary to introduce quarks and gluons into the eikonal formalism, so the parton model is an essential gateway into the microscopic domain of color interactions. Once we enter that domain, we embark on an unconventional journey of studying color mutation of the constituents as a dynamical process by which the colors of the quarks evolve through the emission and absorption of gluons. The smallness of  $\alpha_S$  is never assumed, so the evolution is not perturbative. With all partons taken into consideration globally, we follow the evolution of the configuration in the color space. When the configuration exhibits color neutral subclusters, we allow branching to take place with a possible contraction of the cluster size in accordance to a reasonable rule consistent with confinement dynamics. Successive branching leads

---

\*Present address: Department of Physics, University of Utah, Salt Lake City, UT 84112.

†E-mail address: hwa@oregon.uoregon.edu

to smaller and smaller clusters, until they are finally identified as particles and resonances. The decay of resonances are also taken into account before the final state of an event is determined. Evidently, the model contains many features of soft interaction that are familiar and desirable at a qualitative level. Here we put them on a quantitative basis.

We shall call this model ECOMB, which stands for eikonal color mutation branching. Only the eikonal part overlaps with an earlier model, called ECCO, an eikonal cascade code [7]. Whereas branching is put in by hand in ECCO, it is a consequence of the color dynamics in ECOMB. Since the partons play a fundamental role in this model, it is significantly closer to QCD than any eikonal model on soft hadronic collisions has ever been.

There are a few parameters in the model. They are adjusted to fit a large body of experimental data on low- $p_T$  processes for  $\sqrt{s} \lesssim 100$  GeV. They include  $\sigma_{el}$ ,  $\sigma_{inel}$ ,  $\langle n \rangle$ ,  $C_q$ ,  $dn/dy$ ,  $P_n$ , and  $F_q$  for all  $s$  in the range  $10 < \sqrt{s} < 100$  GeV, and all rapidity intervals.  $F_q$  are the normalized factorial moments, whose power-law dependence on the rapidity bin-size  $\delta$  has been referred to as the intermittency behavior [8]. Except for  $F_q$ , all the other pieces of data are global in nature; i.e., examined in or averaged over all rapidity space. They can be fitted by many models.  $F_q$  in small rapidity intervals exhibit local fluctuations, which are what invalidate most of those models.

There is one important aspect about our model that should be commented on in these introductory remarks. ECOMB is built upon the parton model, and therefore represents an approach to multiparticle production at low  $p_T$  that is opposite to that of the more familiar models, such as the Lund string model [9], and the dual parton model [10]. The basic idea of those models is that the momentum of an incident hadron is carried mainly by a few of the valence quarks, which upon collision drag a color flux tube or a string that subsequently fragment due to confinement forces. The parton model, on the other hand, as originally proposed by Feynman for soft processes [11], regards the hadron momentum as being carried by all partons, whose momentum distribution is frozen by a hard collision process (except for  $Q^2$  evolution). For production at low  $p_T$  the partons cannot be regarded as being momentarily free. It does not mean that the parton model is invalid; it only means that the model cannot be naively applied, as in hard processes. In describing the inclusive cross section of  $pp$  collision in the large  $x_F$  region, the Lund model [9] had one extreme view in that the produced hadrons are the result of string fragmentation, while the recombination model [12] had the other extreme view in that the partons that are originally in the incident hadrons recombine to form the detected hadrons. Whereas the Fritiof model [13] is a refinement of the original Lund model, ECOMB represents an enormous step of upgrading of the original recombination model. Most importantly, it treats hadronization in the central region with due regard to hadron size as well as color dynamics.

The paper is organized as follows. In Sec. 2 we review the Geometrical Branching Model (GBM) with emphasis on the eikonal formalism for multiparticle production. Then the parton model is incorporated into the GBM in Sec. 3. The parton number distribution at each impact parameter is used only as the initial condition for the dynamical evolution process of color mutation, which is discussed in Sec. 4. The comparison of the results from Monte Carlo calculation with the data on intermittency is carried out in Sec. 5. Some concluding remarks are made in the final section.

## II. A REVIEW OF THE GEOMETRICAL BRANCHING MODEL

The aim of GBM is to describe multiparticle production in hadronic collisions through soft interaction [14]. To focus on processes in which hard subprocesses are unimportant, we confine our attention to the energy range  $10 < \sqrt{s} < 100$  GeV, which covers the CERN ISR energies. The model is constructed to possess the properties of geometrical scaling [5] and approximate Koba-Neilsen-Olesen (KNO) scaling [6] that are observed in that energy range. It consists of two parts: the geometrical part that is based on the eikonal formalism of hadronic collisions, and the branching part that describes how hadrons are produced. The details of the later will be modified and improved in the following sections. Here we review the general framework of how the two parts are put together.

In terms of the eikonal function  $\Omega(b)$ , which is assumed known from an independent source, the elastic, inelastic, and total cross sections are

$$\sigma_{el} = \int d^2b (1 - e^{-\Omega(b)})^2 \quad , \quad (1)$$

$$\sigma_{inel} = \int d^2b (1 - e^{-2\Omega(b)}) \quad , \quad (2)$$

$$\sigma_{tot} = \int d^2b 2(1 - e^{-\Omega(b)}) \quad . \quad (3)$$

In the energy range stated above there is geometrical scaling; i.e.,  $\sigma_{el}/\sigma_{tot}$  is roughly constant [5]. That property can be guaranteed, if  $\Omega$  depends only on the scaled impact parameter  $R$ , where

$$R = b/b_0(s) \quad , \quad (4)$$

so that (1)-(3) may be written as

$$\sigma_{el} = \pi b_0^2(s) \int_0^\infty dR^2 (1 - e^{-\Omega(R)})^2 \quad , \quad (5)$$

$$\sigma_{inel} = \pi b_0^2(s) \int_0^\infty dR^2 (1 - e^{-2\Omega(R)}) \quad , \quad (6)$$

$$\sigma_{tot} = \pi b_0^2(s) \int_0^\infty dR^2 2(1 - e^{-\Omega(R)}) \quad . \quad (7)$$

In order that the inelasticity function

$$g(R) = 1 - e^{-2\Omega(R)} \quad (8)$$

satisfies the normalization condition

$$\int_0^\infty dR^2 g(R) = 1 \quad , \quad (9)$$

we are free to set the scale  $b_0(s)$  by requiring

$$\sigma_{inel} = \pi b_0^2(s) \quad . \quad (10)$$

The function  $g(R)$  describes the probability of having an inelastic collision at  $R$ .

The multiplicity distribution  $P_n$  is a result of sampling the multiparticle production processes by many collisional events, each of which may have a different impact parameter. Hence,  $P_n$  should have the form

$$P_n = \int dR^2 g(R) \mathbf{Q}_n(R) \quad , \quad (11)$$

where  $\mathbf{Q}_n(R)$  is the probability of producing  $n$  particles at impact parameter  $R$ . Both  $P_n$  and  $\mathbf{Q}_n$  are normalized by

$$\sum_n P_n = \sum_n \mathbf{Q}_n = 1 \quad . \quad (12)$$

The eikonal formalism is, of course, quite general. It satisfies unitarity, which relates elastic and inelastic scattering amplitudes. Furthermore, it emphasizes the spatial properties of the colliding hadrons, which are known to be extended objects. Any treatment of the collision process that ignores the geometrical aspects of the hadrons leaves out some part of the physics of the problem, which cannot be unimportant for soft processes.

The inelasticity function  $g(R)$ , defined in (8), can be expanded in a power series

$$g(R) = \sum_{\mu=1}^{\infty} \pi_\mu(R) \quad (13)$$

where

$$\pi_\mu(R) = \frac{[2\Omega(R)]^\mu}{\mu!} e^{-2\Omega(R)}. \quad (14)$$

The  $\mu$ th-order term may be regarded as the  $\mu$ th-order rescattering contribution, and can be related to the  $\mu$ -cut-Pomeron [15, 7]. In this paper we use  $\mu$ -cut-Pomeron only as a terminology in reference to the  $\mu$ th term in the expansion (13). For  $\mu \geq 2$ ,  $\pi_\mu$  is small compared to  $\pi_1$  except at small  $R$  for any reasonable  $\Omega(R)$ . For  $pp$  collisions the well-determined form for the eikonal function is [16]

$$\Omega(R) = -\ell n \left( 1 - 0.71 e^{-1.17 R^2} \right), \quad (15)$$

which has been used to give a good description of  $d\sigma/dt$  [17]. To get an estimate of the average  $\mu$ , let us define

$$\bar{\mu}(R) = \sum_{\mu=1}^{\infty} \mu \pi_\mu(R) / \sum_{\mu=1}^{\infty} \pi_\mu(R) \quad (16)$$

and

$$\langle \mu \rangle = \int dR^2 g(R) \bar{\mu}(R) = \int dR^2 2\Omega(R). \quad (17)$$

Using (15) in (17), one gets  $\langle \mu \rangle = 1.6$  [18]. Thus unless  $R \simeq 0$ , high-order terms involving  $\mu > 2$  are negligible. But for the high- $n$  behavior of the multiplicity distribution  $P_n$ , small  $R$  collisions are very important.

As far as the geometrical aspect of the collision problem is concerned, the above discussion summarizes all that is important. To go further in multiparticle production, it is necessary to model the dynamics of soft interaction. Before we enter into the details of that, we consider here the connection between particle production and geometry. At each  $R$ ,  $\pi_\mu(R)$  gives the probability of having  $\mu$ -cut-Pomerons, for which we use  $\mathbf{B}_n^\mu$  to denote the probability of producing  $n$  particles. Thus the overall  $P_n$  is a convolution

$$P_n = \int dR^2 \sum_{\mu=1}^{\infty} \pi_\mu(R) \mathbf{B}_n^\mu \quad (18)$$

with  $\sum_n \mathbf{B}_n^\mu = 1$ . Going back to the general formula (11), it is clear from (18) that  $\mathbf{Q}_n$  is a weighted average of  $\mathbf{B}_n^\mu$ :

$$\mathbf{Q}_n(R) = \sum_{\mu=1}^{\infty} \pi_\mu(R) \mathbf{B}_n^\mu / \sum_{\mu=1}^{\infty} \pi_\mu(R), \quad (19)$$

where (13) has been used.

Using (14) and (15), the dependence of  $\pi_\mu(R)$  on  $R$  is shown in Fig. 1 for various values of  $\mu$ . Evidently, at large values of  $R$  only the  $\mu = 1$  term is important. At  $R \equiv 0$ , terms up to  $\mu = 6$  can still make small contributions. The sum in (13), when truncated at  $\mu = 6$ , is shown by the heavy dashed line in Fig. 1, and well approximates  $g(R)$  shown by the heavy solid line in Fig. 1. Thus we see in (19) that at smaller  $R$  more terms in the sum over  $\mu$  are needed, resulting in more particles produced, as is physically reasonable.

### III. INCORPORATION OF THE PARTON MODEL

In an earlier version of the GBM [7], a self-similar branching process is assumed for  $\mathbf{B}_n^\mu$ , whose  $n$  dependence is determined by simulation. The defect of that approach is that the dynamics of branching is *ad hoc*, not based on QCD. The guiding principle is self-similarity, i.e., a cluster of mass  $m$  branches into two subclusters of masses  $m_1$  and  $m_2$  with probability  $D(m, m_1, m_2)$  that is independent of any specific mass scale. The aim is to reproduce the intermittency phenomenon observed, as the resolution scale is varied [3]. We now want to improve the model by incorporating nonperturbative QCD to the extent feasible. Branching becomes a derived property in the present approach, instead of an assumed property in ECCO [7].

To do so, it is necessary to put the model in a framework in which the interactions of quarks and gluons can be examined in detail, with hadrons being the end product of the hadronization process. Since our aim is to study soft interaction in low- $p_T$  production processes, rigorous calculation from first principles is not possible. Even the use of the parton model may be questionable when the virtuality  $Q^2$  that is relevant to the process is not high. However, bearing in mind that Feynman's first paper on the parton model addresses specifically the soft interaction problem [11], we shall similarly frame our investigation in the language of partons without using perturbative approximations. Indeed, it is because the interactions are soft that we have to follow the time evolution of the partons.

An important departure from the usual application of the parton model is that we combine the property of hadrons being spatially extended objects with the property of hadrons being made up of smaller constituents. Clearly, for most collisions whose impact parameters are nonzero, only portions of the partons in the incident hadrons overlap and interact, so the number of hadrons produced depends on that overlap. The event-to-event fluctuation of the particle multiplicity therefore depends strongly on the impact-parameter fluctuation, and the event averaged parton distributions, as determined from the structure functions, are of no use in that respect.

To implement our amalgamation of the two properties stated above, we adopt the eikonal description of Sec. 2 and modify (19) to refer to parton number instead of hadron number. Thus let us define  $Q_\nu(R)$  to be the probability of involving  $\nu$  partons in soft interaction in the overlap region when the two incident hadrons are separated by a scaled impact parameter  $R$ ; let  $B_\nu^\mu$  be the probability of having  $\nu$  partons in the  $\mu$ -cut Pomeron. Note that we have used  $Q_\nu$  and  $B_\nu^\mu$  in place of  $\mathbf{Q}_n$  and  $\mathbf{B}_n^\mu$ , when we refer to the  $\nu$  partons instead of the  $n$  particles. The parton and particle distributions are, of course, very different. As in (19),  $Q_\nu$  and  $B_\nu^\mu$  are related by

$$Q_\nu(R) = g^{-1}(R) \sum_{\mu=1}^{\infty} \pi_\mu(R) B_\nu^\mu \quad . \quad (20)$$

We emphasize that in (20) the subscripts  $\nu$  refer to the number of partons that initiate the evolution process leading toward the hadrons produced in the central rapidity region. The nonoverlapping portions of the incident hadrons produce the leading particles in the fragmentation regions. If we use  $\mathcal{E}_{\nu \rightarrow n}\{\cdots\}$  to denote the evolution process that takes the  $\nu$  partons to the  $n$  hadrons, we may express the relationship between  $Q_\nu(R)$  and  $\mathbf{Q}_n(R)$  symbolically as

$$\mathbf{Q}_n(R) = \mathcal{E}_{\nu \rightarrow n}\{Q_\nu(R)\} \quad . \quad (21)$$

The description of  $\mathcal{E}_{\nu \rightarrow n}$  is the main task of this paper.

A way of thinking about  $B_\nu^\mu$  is to consider the  $\mu = 1$  case, for which we have a one-Pomeron exchange diagram for the elastic scattering amplitude with the Pomeron being cut to expose the internal lines on mass shell. If the Pomeron is represented by a ladder of gluons with quark loops, then cutting it reveals the gluons, quarks and antiquarks, which constitute the partons of  $B_\nu^1$ . Being the probability (i.e., absolute square of the amplitude for  $p + p \rightarrow \nu$  partons) of having  $\nu$  partons in the one cut-Pomeron,  $B_\nu^1$  is, of course, more general than any specific model approximating that Pomeron by ladders or otherwise. Similarly,  $B_\nu^\mu$  is the corresponding probability, when  $\mu$  Pomerons in the elastic amplitude are cut.

Since there exists no rigorous derivation of  $B_\nu^\mu$ , we shall assume that it is Poisson distributed around some mean number  $\bar{\nu}$  of partons. It is reasonable, since it is known that a cut ladder corresponds to a multiperipheral diagram for a  $\nu$ -particle production amplitude, whose rapidity distribution is uniform, and multiplicity distribution Poissonian. The mean number  $\bar{\nu}(\mu, s)$  can depend on both  $\mu$  and  $s$ , since we expect  $\bar{\nu}$  to increase with  $\mu$  and  $s$ . Lacking any information on that dependence, except that the  $s$  dependence should be logarithmic, this being log  $s$  physics, we adopt the following parameterization

$$\bar{\nu}(\mu, s) = \hat{\nu}(s) \mu^{a(s)} \quad , \quad (22)$$

where

$$\hat{\nu}(s) = \nu_0 + \nu_1 \ln s \quad , \quad (23)$$

$$a(s) = a_0 + a_1 \ln s + a_2 \ln^2 s \quad . \quad (24)$$

We shall use these in

$$B_\nu^\mu = \frac{1}{\nu!} [\bar{\nu}(\mu, s)]^\nu e^{-\bar{\nu}(\mu, s)} \quad , \quad (25)$$

which in turn is used in (20) to determine  $Q_\nu(R)$ .

In the next section we describe the algorithm for parton evolution in color space event by event. For each event we simulate a scaled impact parameter  $R$ . For that  $R$ , we use  $Q_\nu(R)$  to simulate an initial parton configuration involving  $\nu$  partons. After the completion of the evolution process, symbolized by  $\mathcal{E}_{\nu \rightarrow n}$ ,  $n$  particles are produced for that event. Repeated simulation of many such events results in a multiplicity distribution  $P_n$  at each  $s$ , a process expressed analytically by (11). From  $P_n(s)$  we can calculate the average multiplicity  $\langle n \rangle(s)$ , and the standard moments

$$C_q(s) = \langle n^q \rangle / \langle n \rangle^q \quad . \quad (26)$$

We vary the parameters in (23) and (24) to fit the data on  $\langle n \rangle(s)$  and  $C_q(s)$  for  $s$  in the range  $10 < \sqrt{s} < 70$  GeV.

Although the hadronization procedure has not yet been described, we give the result here first to close our discussion on the initial parton distribution. We do this so as not to lose sight of the global features of multiparticle production, when our attention is turned to the local properties in the following sections. The data that we want to fit are  $\langle n \rangle_{\text{ch}}$  and  $C_q$  from Refs. [19]. They are shown in Figs. 2 and 3. The solid lines are our calculated results using

$$\begin{aligned} \nu_0 &= -5.10, & \nu_1 &= 4.03, \\ a_0 &= -1.1, & a_1 &= 0.41, & a_2 &= -0.025, \end{aligned} \quad (27)$$

in (23) and (24) with  $s$  in units of  $\text{GeV}^2$ . The relative  $s$ -independence of  $C_q(s)$ , which is a manifestation of the KNO scaling, is nontrivial when  $\langle n \rangle(s)$  more than doubles over the energy range considered for soft production only. The fits in Figs. 2 and 3 are evidently very satisfactory.

Before we go into the details of the color dynamics that is responsible for the calculated results, let us show the parton number distributions  $Q_\nu(R)$ . They are plotted in Fig. 4 for four representative values of  $R$  and for  $\sqrt{s} = 52$  GeV. Note that the peak does not move below  $\nu = 25$ , as  $R$  is increased; it is due to the fact that the minimum  $\nu$  is 1, no matter how large  $R$  is. Note also that the typical parton numbers are not large by the standards of hard processes at much higher energies. That is connected with the nature of those partons that initiate the evolution process, a subject we turn to next.

#### IV. COLOR MUTATION

We now consider the color dynamics of soft interaction. The initial state is that there are  $\nu$  partons distributed in some fashion in a linear array in rapidity space. This is a consequence of the parton model in that the partons are in the incident hadrons to begin with, and the collision rearranges those partons and sets off the evolution process that takes those partons to the final state, where the produced hadrons are decoupled. The evolution process involves quarks and antiquarks emitting and absorbing gluons. Since the process is not perturbative, there is no analytical method to track the time development of the process. Thus we shall use Monte Carlo simulation to generate the configuration at each time step.

There are two spaces in which we must track the motion of the color charges. One is the two-dimensional color space; the other is the one-dimensional rapidity space. The latter can be extended to include the azimuthal angle  $\phi$  and the transverse momentum  $|\vec{p}_T|$ , but in our first attempt here we integrate over those variables and examine the simpler problem of a 1D system. As for the color space, it is 2D, and can be spanned by the  $(I_3, Y)$  axes, as in  $SU(3)$  flavor. The configuration in the two spaces are coordinated in the following sense. Starting from the extreme left end of the rapidity ( $\eta$ ) space, for which the system that contains no partons is by definition color neutral and therefore is represented by a point at the origin of the color space, we move in the positive direction in  $\eta$  space until we cross a color charge. At the point to the right of that color charge, the corresponding point in the color space jumps from the origin to a position that represents the color of the charge that has been crossed. Let us denote that jump by a vector. Then each time we cross a color charge in the  $\eta$  space, there is a corresponding vector added to the previous point in the color space. The succession of additions of those vectors, each one starting from the tip of the previous

one, forms a path. Since the whole parton system is color neutral, by the time we have moved to the extreme right in the  $\eta$  space, the path in the color space returns to the origin, thus forming a closed loop. Such a loop may be self-intersecting at various points. We call such a closed path a configuration of the system in color space.

The essence of our evolution process is to track the configuration of the system at each time step. The configuration changes because the colors of the partons can mutate, as they interact through the emission and absorption of gluons. The way that each color charge mutates is determined by the use of an energy principle, which is proposed on the grounds that the system attempts to lower its energy by changing its color configuration, but fluctuating forces at the microscopic level cause the changes to be erratic. At the same time, the confinement force tends to reduce the distances among the color charges, which are separated initially because of the initial momenta that the partons possess, while being constituents of the incident hadrons. Since we work in the 1D  $\eta$  space and cannot use perturbative QCD, we do not treat the scattering problem among the partons in either the momentum or the coordinate space. The evolution of the configuration in the color space is what is important.

When the closed path in the color space evolves to a configuration in which the path crosses the origin, a point in the evolution is then reached that requires special attention. At that point, the configuration may be regarded as having two closed paths, corresponding to two color neutral subsystems. We assume that a subsystem with no net color charge (i.e.  $I_3$  and  $Y = 0$  in color space) is in the lowest  $SU(3)$  representation, that is, a singlet. This assumption is based mainly on the expectation that a nonsinglet system requires more energy to sustain it than a singlet system. Relaxation to the lowest energy state, despite fluctuations, is the principle that guides the evolution. Since two spatially separate singlet subsystems do not interact, we regard a branching process to have taken place: the original large cluster of partons has partitioned itself into two smaller color neutral subclusters. Thereafter, we repeat our procedure of color mutation, but now applied to the two subclusters separately. This process is repeated again and again until all subsystems consist of only quark-antiquark pairs that cannot branch any further. However, a  $q\bar{q}$  subsystem can be a resonance, in which case it can decay into pions and kaons.

So far, we have described only qualitatively the evolution process of color mutation and branching. The quantitative implementation of the procedure will be given below. The conceptual basis of our approach to soft production incorporates many features of strong interaction that are generally regarded as being reasonable and physical, but lacking calculational schemes with results for comparison with data. We now amend that defect. The procedure that we adopt to carry out the calculations is not unique, and can be modified and improved in time. But the framework of ECOMB is fixed by the combination of eikonalism, color mutation, and branching. Our present procedure is as follows.

### A. Initial Distributions of the Partons

As described in Sec.3, we start out with  $\nu$  partons for a given event. It is a number generated by use of the eikonal formalism with variations in the impact parameter taken into account. How the  $\nu$  partons are distributed in rapidity is drawn from the parton model. An important basis of our model is that partons are in the incident hadrons before the collision, and are not to be regarded as  $q\bar{q}$  pairs that are excited from the vacuum due to the stretching of strings in the string model. Thus our partons have a momentum-fraction distribution as determined in leptonproduction, but with  $Q^2$  as small as can be achieved.

In the parton model there has always been a question of how gluons hadronize in low- $p_T$  processes, when the produced particles are predominantly pions. In the recombination model for particle production in the fragmentation region [12], the problem is handled by saturating the sea, i.e., by converting all gluons to quarks and antiquarks at the outset. The normalization of the hadronic inclusive cross section turns out to be correct, when the recombination mechanism is applied to all quarks and antiquarks that are nearby in phase space. We now use the same saturation of the sea in our problem here, as we attempt to treat the central region. Thus when we refer to partons in the following, we shall mean only quarks and antiquarks. The  $\nu$  partons are therefore color triplets and antitriplets of equal numbers so that collectively they form a color neutral system. Their distributions in rapidity and color spaces are to be considered separately.

(1) *Distribution in rapidity space*

By rapidity we mean space-time rapidity  $\eta$ , where

$$\eta = \frac{1}{2} \ell n \frac{t+z}{t-z} . \quad (28)$$

Momentum rapidity  $y$  will not be used throughout the calculation until the end, when the momentum of a produced particle is to be determined. We use the  $\eta$  variable because the spatial separations between partons change during the evolution process due to the color forces.

The usual parton distribution in momentum fraction (at the lowest accessible  $Q^2$ ) implies roughly a flat  $\eta$  distribution with rapid damping toward zero at large  $\eta$ . We approximate that distribution for the forward-going incident hadron by

$$\begin{aligned} \rho^{(f)}(\eta) &= \rho_0 , & 0 \leq \eta \leq \eta_c , \\ \rho_0 \frac{\eta_{\max} - \eta}{\eta_{\max} - \eta_c} , & & \eta_c \leq \eta \leq \eta_{\max} , \end{aligned} \quad (29)$$

where  $\rho_0 = \nu/(\eta_{\max} + \eta_c)$ , which corresponds to a total of  $\nu/2$  partons when integrated over  $\eta > 0$ . For the partons belonging to the backward-going incident hadron, the  $\eta$ -distribution is

$$\begin{aligned} \rho^{(b)}(\eta) &= \rho_0 , & -\eta_c \leq \eta \leq 0 , \\ \rho_0 \frac{\eta_{\max} + \eta}{\eta_{\max} - \eta_c} , & & -\eta_{\max} \leq \eta \leq -\eta_c . \end{aligned} \quad (30)$$

The partons in each of  $\rho^{(f)}$  and  $\rho^{(b)}$  should add up to be color neutral. The overall parton distribution in the initial state is then

$$\rho(\eta) = \rho^{(f)}(\eta) + \rho^{(b)}(\eta) . \quad (31)$$

For each event, the partons are, to first approximation, distributed randomly in  $\eta$  according to  $\rho(\eta)$ .

The above distribution describes the rapidities of the partons before the collision of the incident hadrons. Upon collision those partons interact, even if only softly. The conventional wisdom about soft interaction is that the range of interaction in rapidity is short. That follows from the known fact that the correlation between produced particles is short-ranged. Thus apart from a limited range ( $-\eta_0 \leq \eta \leq \eta_0$ ) in the central region where the partons from the two incident hadrons interact, most partons outside that range are undisturbed by the collision. We describe the effect of the interaction by modifying the initial distributions  $\rho^{(f)}(\eta)$  and  $\rho^{(b)}(\eta)$  in that interaction region to  $\rho^{(1)}(\eta)$  and  $\rho^{(2)}(\eta)$ , respectively, where

$$\rho^{(1)}(\eta) = \rho_0 \frac{\eta + \eta_0}{2\eta_0} \theta(\eta + \eta_0) \theta(\eta_0 - \eta) + \rho^{(f)}(\eta) \theta(\eta - \eta_0) , \quad (32)$$

$$\rho^{(2)}(\eta) = \rho_0 \frac{-\eta + \eta_0}{2\eta_0} \theta(\eta + \eta_0) \theta(\eta_0 - \eta) + \rho^{(b)}(\eta) \theta(-\eta - \eta_0) . \quad (33)$$

Note that the total parton distribution is unchanged, i.e.,

$$\rho^{(1)}(\eta) + \rho^{(2)}(\eta) = \rho(\eta) . \quad (34)$$

The shapes of  $\rho^{(1)}(\eta)$  and  $\rho^{(2)}(\eta)$  are now trapezoidal: some of the partons initially between  $\eta = 0$  and  $\eta_0$  in  $\rho^{(f)}(\eta)$  are dragged to the negative  $\eta$  region, and some between  $\eta_0$  and 0 in  $\rho^{(b)}(\eta)$  are dragged to the positive  $\eta$  region. Fig. 5 illustrates how the distributions look like at a low energy where the trapezoids are almost triangular. This rearrangement may not seem significant for the inclusive cross section of the produced hadrons, since  $\rho(\eta)$  is unchanged, but it turns out to be important for multiplicity fluctuations in smaller bins. The point is that  $\rho^{(f)}$  and  $\rho^{(b)}$  are two color-neutral clusters, coming from the two incident hadrons. The rearrangement caused by the collision creates an overlapping region so that there is no smaller segment within the entire range,  $-\eta_{\max} \leq \eta \leq \eta_{\max}$ , where one can find color neutrality, except by accident. The color mutation process is sensitive to the fact that the partons distributed according to  $\rho^{(1)}(\eta) + \rho^{(2)}(\eta)$



has no color-neutral subclusters, so that the evolution must begin from the whole cluster, not from the two neutral subclusters,  $\rho^{(f)}$  and  $\rho^{(b)}$ , separately.

One can find a rough parallel between our  $\rho^{(1,2)}(\eta)$  and the strings in the Fritiof model [13] or in the dual parton model [10]. However, a string in DPM is stretched between a quark in one incident proton with a diquark in another proton. Our  $\rho^{(1)}(\eta)$  is a color-neutral cluster of partons distributed from  $-\eta_0$  to  $\eta_{\max}$ .

To summarize, whereas  $\rho^{(f)}(\eta)$  and  $\rho^{(b)}(\eta)$  are the initial parton distributions of the incident hadrons,  $\rho^{(1)}(\eta)$  and  $\rho^{(2)}(\eta)$  are the parton distributions after the hadrons pass through the interaction region. The evolution of the color dynamics begins thereafter starting with  $\rho^{(1)}(\eta)$  and  $\rho^{(2)}(\eta)$ .

## (2) Distribution in color space

In the color space spanned by  $I_3$  and  $Y$ , a quark is represented by a vector, which has the coordinates of one of the triplets:  $(1/2, 1/3)$ ,  $(-1/2, 1/3)$ , and  $(0, -2/3)$ . An antiquark is represented by a vector directed opposite to one of the above. As a distribution of partons in the  $\eta$  space is generated, say,  $\rho^{(2)}(\eta)$  between  $-\eta_{\max} \leq \eta \leq \eta_0$ , we assign to each parton a color vector consistent with the requirement that the quarks and antiquarks come in pairs, but their orderings in the  $\eta$  and the color spaces are totally random. The partons in  $\rho^{(1)}(\eta)$  are distributed similarly, but completely independently, between  $-\eta_0 \leq \eta \leq \eta_{\max}$ . The total distribution  $\rho(\eta)$  in  $-\eta_{\max} \leq \eta \leq \eta_{\max}$  is the sum of these two sets, whose partons are merged in the  $\eta$  and the color spaces. Thus as we move from the extreme left in the  $\eta$  space in the  $+\eta$  direction, we begin at the origin of the color space, and, each time when we move over a parton in the  $\eta$  space, we add a vector (corresponding to its color) with its tail to the head of the previous vector (or to the origin if it is the first parton). A succession of such vectors forms a trajectory in the color space. The trajectory eventually ends at the origin, thus forming a closed path, when  $\eta$  reaches the extreme right.

Note that the path in the color space is dual to the “path” in the 1D  $\eta$  space in the sense that the segment between two partons in the  $\eta$  space is mapped to a point in the color space, while the point where a parton is located is mapped to a segment of the path in the color space. Thus the closed path is made up of  $\nu$  short segments. An example of a path in color space is shown in Fig. 6. The sequence of color charges represented by the vectors is indicated by  $r\bar{b}rg \cdots \bar{b}r$  in the figure. We have used the notation  $r = (1/2, 1/3)$ ,  $g = (-1/2, 1/3)$ , and  $b = (0, -2/3)$ . The origin is labeled by 0.

## B. Evolution in the color and rapidity spaces

We now consider the evolution of a configuration due to QCD dynamics. A nonperturbative treatment of  $\nu$  simultaneously interacting color charges is, of course, too difficult to contemplate here. We reduce the problem by considering pairwise near-neighbor interaction via the exchange of a gluon in any of the  $s$ -,  $t$ -, or  $u$ -channel, whichever is applicable. Starting from the extreme left in the  $\eta$  space, we regard the ordered chain of  $\nu$  partons as having  $\nu - 1$  links (with varying link lengths). Its dual path in the color space has  $\nu$  vectors, meeting at  $\nu - 1$  vertices, not counting the endpoints, which are located at the origin. Pairwise near-neighbor interaction means that we consider the  $\nu - 1$  links in  $\eta$  space one at a time, according to a rule to be specified below. After the interactions at all  $\nu - 1$  links are considered, the evolution of the whole configuration is regarded as having taken one time step, and the process is then repeated.

### (1) Color interaction

Consider any link in the chain, i.e., a pair of partons. Suppose that the pair is  $(r, \bar{g})$ . The only possible outcome of an interaction by the emission and absorption of a gluon, besides remaining as  $(r, \bar{g})$ , is  $(\bar{g}, r)$ , since the sum of the two color vectors must remain invariant. If the pair consists of quarks, such as  $(r, g)$ , the only outcome of an interaction is again either  $(r, g)$  or  $(g, r)$ . Only in the case of a color-neutral pair, such as  $(r, \bar{r})$ , can the outcome be any such pair, i.e.,  $(r, \bar{r})$ ,  $(g, \bar{g})$ ,  $(b, \bar{b})$  or their exchanged pairings. To determine the specific outcome of an interaction, we use a statistical method.

For every global configuration  $\alpha$  of the  $\nu$  partons, there is an associated energy  $E_\alpha$ . How  $E_\alpha$  is determined will be described in the following subsection. Whenever a local pair of partons interact, the outcome may or may not affect the global configuration. Let  $c$  be the total number of possible configurations. From the

foregoing discussion  $c$  can only be 2 or 6, the latter being for a color-neutral pair. Our statistical approach to the determination of the global configuration  $\alpha$ , consistent with favoring the lowest energy state, requires that the probability for configuration  $\alpha$  to occur is

$$P_\alpha = e^{-\beta E_\alpha} / Z, \quad Z = \sum_{\alpha=1}^c e^{-\beta E_\alpha}, \quad (35)$$

where  $\beta$  is a free parameter.

Using the Metropolis algorithm, we use  $P_\alpha$  to determine the outcome of a local interaction at every link. The result affects only one vertex of the closed path in the color space, one vertex at a time. As we go down the chain, every vertex is then tested for possible changes. At the end of one complete sweep for one time step, the whole closed path has undergone a color mutation, resulting in a new path. Note that our procedure incorporates several features of the dynamics governing the system. Locally, there is the QCD dynamics of gluon exchange between quarks and antiquarks. The outcome of the local interaction depends on the global configuration in the color space. The statistical treatment takes into account the fluctuating nature of the many-body problem.

## (2) Energy of a color configuration

The color mutation process is an attempt by the dynamical system to relax to its lowest energy state. It starts initially at a high energy state because the collision puts the partons in a spatially spread-out domain by virtue of the initial momenta of the partons that are essentially uninterrupted by the soft collision, i.e., no large momentum transfers. Color charges that are dispersed in space have high potential energy. Since soft interactions do not result in significant changes in the parton momenta, the energy of the system is controlled mainly by the potential energies residing at all the links in the  $\nu$ -parton chain.

Specifically, consider the  $i$ th link in a chain, where  $i = 1, 2, \dots, \nu - 1$ . The net color charge that the link sees on the left side is

$$\vec{C}_i = \sum_{j=1}^i \vec{c}_j, \quad (36)$$

where  $\vec{c}_j$  is the vector in color space representing the color of the  $j$ th parton. Due to the color neutrality of the whole system, the net color that the link sees on the right side is  $-\vec{C}_i$ . Since the potential energy at the link  $i$  is proportional to the net color charges on the two sides of the link, we write the energy  $E_i$  of the  $i$ th link in the simple form

$$E_i = \left| \vec{C}_i \right|^2, \quad (37)$$

where the proportionality factor is absent for the following reason. The confinement potential should be proportional to the distance between color charges. Here  $\vec{C}_i$  is the total color of all the partons to the left of the  $i$ th link, so the relevant effective distance should be measured from the center of those partons on the left side to the center of the partons on the right side. That is a global distance that is roughly half the total  $\eta$  range, insensitive to the position of the  $i$ th link. Since  $E_\alpha$  is never used without  $\beta$  in (35), the omission of the proportionality factor in (37) is equivalent to letting it be absorbed in the definition of  $\beta$ . The energy associated with the whole configuration  $\alpha$  is

$$E_\alpha = \sum_{i=1}^{\nu-1} E_i, \quad (38)$$

where the sum obviously depends on the particular path in color space that the configuration  $\alpha$  takes.

It is this energy  $E_\alpha$  in (38) that the system attempts to lower by color mutation, as it changes from one configuration  $\alpha$  to another,  $\alpha'$ . Because of the additive nature of  $E_\alpha$  in (38), the probability of mutation is determined by the local energy difference, as can be seen in the following example. Consider a link for which the number of possible configurations is two, i.e.,  $c = 2$  in (35). Then  $P_\alpha$  can be written as

$$P_\alpha = \frac{1}{1 + e^{-\beta \Delta E}}, \quad (39)$$

where  $\Delta E$  is the change of energy in going to the new configuration  $c'$

$$\Delta E = E_{\alpha'} - E_\alpha = E'_i - E_i. \quad (40)$$

$E'_i$  is the energy at the  $i$ th link in the new configuration. Note that  $\Delta E$  is now locally determined at the link  $i$ . However, the energy  $E_i$  and  $E'_i$  depend on the global configurations in the color space, due to (36) and (37).

Since the net color charge of all the partons on one side of a link can be large,  $E_i$  can also be large, according to (37). Thus unless  $\beta$  is a small number, (39) can give a probability distribution  $P_\alpha$  that can have an abrupt change at  $\Delta E = 0$ . To round off the edges,  $\beta$  would have to be quite small.

### (3) Spatial fluctuations

The length of the  $i$ th link in the  $\eta$  space is

$$d_i = \eta_{i+1} - \eta_i, \quad (41)$$

where  $\eta_i$  is the rapidity of the  $i$ th parton, counting from the left at  $\eta = -\eta_{\max}$ . For a spatially extended color-neutral system, we have positive link lengths,  $d_i \geq 0$ . We put  $d_i = 0$ , when two partons are in the same  $\eta$  bin. The rapidity range,  $-\eta_{\max} \leq \eta \leq \eta_{\max}$ , is divided into 256 bins in our numerical calculation, so the smallest bin size is  $2\eta_{\max}/256$ , which, of course, depends on the collision energy. As far as the problem regarding the spatial distribution is concerned, we shall assume energy independence and work only in the space that has 256 basic units, whatever  $\eta_{\max}$  is. We denote the width of the basic unit by  $\delta\eta$ .

On the basis of (35) and (37) the system undergoes color mutation, as it evolves toward the final state. In addition to the fluctuation of the color charge  $\vec{C}_i$ , the length of the  $i$ th link,  $d_i$ , which is an integer in units of  $\delta\eta$ , can also fluctuate. Whether the link length contracts or expands depends on the attractiveness or repulsiveness of the net color forces that act on the two ends of the link. To determine the nature of that force is beyond the scope of this treatment. We shall model the change in link length by a stochastic approach, consistent with how we have handled the color mutation part of the dynamics of the complex system. We allow  $d_i$  to change by an integer  $m_i$ , i.e.,  $d_i \rightarrow d_i + m_i$ , where the probability for  $m_i$  is specified by a distribution  $\mathcal{P}_i(m)$ . Apart from the consideration that a contraction cannot render  $d_i$  negative, we would set  $\mathcal{P}_i(m)$  to be a uniform distribution from  $-m_-$  to  $m_+$ , where  $m_\pm \geq 0$ . However, if  $m_- > d_i$ , we truncate  $\mathcal{P}_i(m)$  at  $m = -d_i$  and place the probabilities for contraction from  $-d_i$  to  $-m_-$  at  $m = -d_i$ . Thus our two-parameter formula for  $\mathcal{P}_i(m)$  can be rewritten in the form that has a constant term plus a Kronecker delta term at  $-d_i$ . That is, with  $\gamma_1$  and  $\gamma_2$  as the two revised parameters, we have

$$\mathcal{P}_i(m) = \gamma_1 \theta(m + d_i) \theta(\gamma_2 - m) + [1 - \gamma_1(\gamma_2 + d_i)] \delta_{m, -d_i}, \quad (42)$$

which satisfies  $\sum_{m=-d_i}^{\gamma_2} \mathcal{P}_i(m) = 1$ . This distribution allows  $m$  to be positive (expansion) uniformly up to  $\gamma_2$ , and negative (contraction) down to  $-d_i$ . The net probability for expansion is  $\gamma_1\gamma_2$ , and for contraction is  $1 - \gamma_1\gamma_2$ .

Confinement implies that there should be a net contraction between the subcluster of charge  $\vec{C}_i$  and the opposite subcluster of charge  $-\vec{C}_i$ . However, these two subclusters are at an effective distance much larger than  $d_i$ , which is the length of the link specifying the separation between the boundaries of the two subclusters. At the  $i$ th link, there are microscopic color forces that can be attractive or repulsive.  $\mathcal{P}_i(m)$  is a two-parameter description of that stochastic force, which should lead to a net macroscopic contraction for the whole cluster. That property is related to the value  $\gamma_1\gamma_2$ , which should be less than 0.5, if contraction dominates over expansion. Of course, this change of  $d_i$  should be tested at all links in the neutral cluster before a net effect is known.

### C. Branching

As we have discussed in the introduction of this section, the evolution process described here is a branching process. A fission of the color-singlet cluster occurs, when it contains two color-singlet subclusters, since

no confining force exists between them. The partitioning takes place when the closed path of the mother cluster evolves to a configuration where the path passes through the origin in the color space so that there are two color neutral subsystems. Thereafter, the color mutation process is applied to the two subsystems separately and independently. This is repeated again and again until all subclusters consist of only  $q\bar{q}$  pairs.

During color mutation, it is possible that a baryon-like singlet can be formed with a  $(r, g, b)$  closed loop. Since baryon-antibaryon pair production in  $pp$  collision is rare at energies where soft interaction is dominant, we shall ignore  $3q$  and  $3\bar{q}$  singlets, (since mass inhibition is not explicitly taken into account), and require color mutation to continue until only mesons are produced. If in the middle of a color chain there is a color neutral  $q\bar{q}$  pair, such as  $r\bar{r}$ , it is not allowed to break off from the chain; it must continue to mutate until a genuine neutral subcluster, counting from the extreme left or right in the  $\eta$  space, is formed.

In Fig. 7 we show an example of how 24 partons evolve under color mutation, and how branching takes place. Thirty-two time steps are taken to get to the final state of  $q\bar{q}$  subclusters only, when hadronization occurs.

To gain some insight on how long a typical evolution process takes for a cluster to partition into two, we show in Fig. 8(a) the distribution in time steps for  $10^3$  initial clusters each consisting of ten pairs of  $q\bar{q}$  with random color ordering. The average is about 3.5 steps for just one branching. For the evolution processes to complete, the daughter clusters must continue to branch successively, and the overall distribution at the end of the evolution is shown in Fig. 8(b). Note that on the average quite a large number of time steps is required for the evolution of an average-sized cluster, much larger than what is usually involved in a hard process where high virtuality is degraded by branching.

At every stage of the evolution process, a cluster shrinks due to overall spatial contraction. We always keep the center of the cluster invariant to conserve momentum. When a branching occurs, the two daughter clusters will have their own respective centers, which will remain invariant during contraction, until they themselves branch. At the end when a hadron is formed from a  $q\bar{q}$  pair, the hadron momentum rapidity  $y$  will be identified with a value of  $\eta$  taken randomly between the  $\eta$  values of the quark and antiquark. The reason for doing this is that without knowing the mass and the transverse momentum  $p_T$  of the hadron, a precise determination of its  $y$  is not possible, nor meaningful. A random value within a small range is good enough. A rough identification of  $y$  with  $\eta$  is justified for free particles at high energy. We do not expect that our measure of fluctuations in the final result will be sensitive to this  $y$ - $\eta$  identification.

#### D. Hadronization

The branching process terminates, when all the neutral subclusters are reduced to the composition of  $q\bar{q}$  pairs only. Those subclusters are identified as hadrons, which may be pions, kaons, or resonances. Those resonances must be allowed to decay before the total number and distribution of particles are counted for the final state of the event. The probabilities of producing various resonances and stable (in strong interaction) particles have been studied experimentally in  $pp$  collisions in [20]. We use that reference as a generic guide for the proportions of all particles produced in any general hadronic collision.

In our simulation we use that guide to determine whether a neutral subcluster is a resonance or not. In either case we give it a transverse momentum according to a specified distribution. Let us use  $k_T$  to denote the transverse momentum of a  $q\bar{q}$  pair. The distribution we use is

$$\frac{dn}{dk_T^2} = \frac{1}{\langle k_T^2 \rangle} e^{-k_T^2 / \langle k_T^2 \rangle} \quad , \quad (43)$$

where  $\langle k_T^2 \rangle$  is a parameter to be varied. If the  $q\bar{q}$  pair forms a pion or a kaon, then that  $k_T$  becomes the  $p_T$  of the particle without any change. However, if the  $q\bar{q}$  pair forms a resonance, then we assume an isotropic decay distribution in the rest frame of the resonance. The azimuthal angle  $\phi$  of  $\vec{k}$  is assigned randomly. After boosting back to the cm system, the 3-momenta  $\vec{p}$  of the decay particles are then determined. The collection of all the final-state particles results in the exclusive distribution in the  $(y, \vec{p}_T)$  space for the event generated.

The charges of the particles are chosen randomly subject to the constraint that the total charge can only be either 0, 1, or 2, on the grounds that the leading particles in a  $pp$  collision can be doubly-, singly-, or un-charged. The particles that we treat are all the produced particles, excluding the leading particles. Once the charge of a specific particle or resonance is generated, the decay of the resonance is then assigned the usual branching fractions into different channels according to the particle data book.

## V. RESULTS

In the previous section we have introduced seven parameters:  $\eta_c$  and  $\eta_{\max}$  in (29) and (30),  $\eta_0$  in (32) and (33),  $\beta$  in (35),  $\gamma_1$  and  $\gamma_2$  in (42), and  $\langle k_T^2 \rangle$  in (43). They are to be varied to fit the data on inclusive distributions and on fluctuations of the exclusive distributions. The properties of fluctuations will be quantified in terms of the normalized factorial moments,  $F_q(\delta)$  for various bin sizes  $\delta$ .

The parameters  $\eta_c$ ,  $\eta_{\max}$ , and  $\langle k_T^2 \rangle$  are essentially kinematical; they set the boundaries of the phase space in which the partons are placed. They do not affect the dynamics of color mutation and the spatial fluctuation of the clusters. The data used to determine them are the rapidity distribution  $dn/dy$  [21] and the transverse momentum distribution  $g(p_T)$  of the produced particles in the final state. The energy range of the data in [21] is  $22 < \sqrt{s} < 63$  GeV, for which hard scattering is negligible. The values of  $\eta_c$  and  $\eta_{\max}$  depend on  $s$ . To fit the data, we have used the values given in Table I. The value of  $(\langle k_T^2 \rangle)^{1/2}$  is chosen to be 400 MeV. In Fig. 9 we show the rapidity distributions where the histograms are the results of our calculation, while the data are from [21]. There,  $\eta$  refers to pseudorapidity, not space-time rapidity. The agreement is clearly satisfactory. Although in carrying out our calculation the other parameters need to be specified also, we have not given them in Table I because the results on  $dn/d\eta$  are insensitive to them. They will be given below.

$\sqrt{s}$	22.0	23.6	30.8	45.2	53.2	63.2
$\eta_c$	1.76	1.55	1.42	0.889	0.762	0.635
$\eta_{\max}$	5.0	6.6	6.6	6.5	6.5	6.5

TABLE 1. The parameters for the initial condition of partons in the evolution

The multiplicity distribution at  $\sqrt{s} = 22$  GeV is shown in Fig. 10 for  $|y| < 2.5$ . The calculated result evidently agrees very well with the data [22], especially at the high  $n$  end. At the low end, there is a slight discrepancy, which could very well be due to the fact that we have not included diffractive production. That portion of the distribution will have negligible effect on our calculation of the factorial moments. We have not included in Fig. 10 the  $P_n$  for narrow rapidity windows, since essentially the same physical content will be conveyed by the  $F_q(\delta)$  to be presented below. We have not considered the UA1 and UA5 data at higher energies because those data contain significant contributions from hard subprocesses. The inclusion of such perturbative processes is not difficult [23,24], and should be investigated in order to extend the energy range where ECOMB can be applied.

The parameters that influence the evolution process of mutation and branching are  $\eta_0$ ,  $\beta$ ,  $\gamma_1$  and  $\gamma_2$ .  $\eta_0$  specifies the overlap region of the initial color-neutral clusters,  $\beta$  pertains to the probability of color mutation, and  $\gamma_1$  and  $\gamma_2$  characterize the fluctuations of the link lengths. The data used to determine them are on factorial moments and their variants [3]. It is here that we can underline the importance of those data on fluctuations, without which we have no guidance on how to restrict the detail dynamics of particle production. Putting that in another way, in the absence of a procedure to calculate from first principles, any model that fails to fit the fluctuation data is missing some aspect of the basic dynamics. To the extent of our awareness, very few models on soft interaction have been put to the test of confronting those data on the factorial moments for varying bin sizes.

The normalized factorial moments, first suggested by Białas and Peschanski [8], can be expressed as

$$F_q = \frac{1}{M} \sum_k \frac{\langle n(n-1)\dots(n-q+1) \rangle_k}{\langle n \rangle_k^q}, \quad (44)$$

where  $n$  is the multiplicity in a bin of size  $\delta$ , the average is performed over all events for the  $k$ th bin, and the summation is over all bins of the same  $\delta$ ,  $M$  being the total number of bins ( $2Y/\delta$ ). Data on  $F_q$  for soft interaction have been obtained by NA22 [25]. In recent years Bose-Einstein correlation between identical particles has been recognized as having an important effect on the intermittency data at very small  $\delta$  [3]. However, at this stage of our development of ECOMB, we have not included BE correlation, since it is unrelated to the color dynamics that we attempt to tune. We therefore limit our scope in this first attempt and focus here on  $F_q$ , for which we fit the data of [25] as functions of bin width, rather than on correlation functions at very small momentum-difference squared.

The parameters that we have varied to give the best fit of the intermittency data at  $\sqrt{s} = 22$  GeV are:

$$\hat{\nu}(s) = 9.1, \quad a(s) = 0.63, \quad (45)$$

$$\eta_{\max} = 5, \quad \eta_c = 3.5, \quad \eta_0 = 1.9, \quad (46)$$

$$\beta = 0.0015, \quad \gamma_1 = 0.077, \quad \gamma_2 = 5. \quad (47)$$

Note that  $\gamma_1\gamma_2 = 0.385$ , implying that it is roughly twice as likely for a link to contract than to expand. To explain why the first four parameters listed above are different from the ones used previously for the ISR data (in Sec. 3 and Table I), we remark that we have not been able to derive from the values of  $F_q$  given by the data of NA22 [25] the values of  $C_q$  that can agree with those of ISR [19]. Thus while the parameters in Table I are adequate for the ISR data that range up to 63 GeV, we must use a slightly different set of parameters at  $\sqrt{s} = 22$  GeV for the NA22 data that provide the only information on intermittency.

In Fig. 11 we show the intermittency data of [25], which to our knowledge have not been reproduced by any model, except ECCO [7,3]. The lines shown in Fig. 11 are the result of our present calculation in ECOMB. Evidently, the agreement between our results and the data are satisfactory for all values of  $\delta y$  and  $q$ . It should be noted that to achieve the fits attained is highly nontrivial. If any part of the dynamical process in generating the hadrons is altered, one would not be able to obtain the rising factorial moments, no matter how many parameters are used. By working with the many parts of our model, all of which affect the determination of  $F_q$ , we have gained confidence in regarding the dynamics of color mutation and branching as having captured the essential properties of soft interaction.

## VI. CONCLUSION

It is rather satisfying that we have been able to reproduce the intermittency data in Fig. 11. Scaling behavior of that type implies self-similarity in the dynamics of particle production. The branching process of color-neutral clusters, successively partitioning into small clusters, is self-similar, since the same algorithm is used at every step. Thus from the outset ECOMB has a chance of generating a scaling behavior, in contrast to the string model or dual parton model, which have been shown by NA22 not to fit the intermittency data [25]. However, to have self-similar dynamics does not guarantee that the observed scaling behavior can be obtained. An appropriate balance of contraction and expansion of the clusters during the evolution is necessary to capture the essence of the color dynamics of a complex system. Furthermore, the initial state of the parton system at the start of the evolution process is also important, since it can dictate the bin size from which the scaling behavior commences. These physical aspects of the model must be incorporated properly in order to produce the result shown in Fig. 11.

We have not considered the intermittency data of UA1 [26] because they contain minijets. If one is willing to adopt the point of view that such semihard subprocesses are not dominant enough to alter the nature of intermittency, one could attempt to apply ECOMB to the UA1 data. However, it is well known that geometrical scaling and KNO scaling are violated at the SPS energies, so some modification is necessary.

The most important omission in this paper is Bose-Einstein correlation, without which our model is not completely realistic. That defect must be corrected in an improved version. At this stage we can only offer this version as a first step in the right direction. Whereas the details of our parametrization here may alter after the BE correlation is incorporated, the branching dynamics of color mutation will hold as the basic framework of the model. Since the power-law behavior of  $F_q$  has been observed for nonidentical particles [27], we know that self-similarity is necessary in the absence of BE correlation. After the symmetrization of identical-particle states is performed, the strength of intermittency may be enhanced. The parameters may therefore have to be readjusted, but the main features of the dynamics need no modification.

We have amalgamated many concepts that form various elements of the conventional wisdom about soft interaction. They include: (a) hadrons having sizes, (b) eikonalism, (c) parton model, (d) interaction of quarks via gluons, (e) statistical properties of a many-body system, (f) spatial contraction and expansion of a color system, and (g) resonance production. They are interlaced by intricate connections described in this paper. One may regard the approximation of nonperturbative QCD by color mutation as a gross simplification. We conjecture that the final realistic result will be insensitive to the details of how well many-body QCD is approximated, since the model is constrained by so many other aspects of soft interaction. This work demonstrates the importance of how each and every one of those separate components of the overall structure must work together in order to achieve the scaling behavior of local fluctuations that is observed.

### Acknowledgment

We are grateful to Prof. W. Kittel for supplying us with the NA22 data and valuable answers to our questions. This work was supported in part by U.S. Department of Energy under Grant No. DE-FG03-96ER40972.

- 
- [1] P. Carruthers, *Hadronic Multiparticle Production* (World Scientific, Singapore, 1988).
  - [2] R.C. Hwa and Q.B. Xie, *Multiparticle Production* (World Scientific, Singapore, 1988).
  - [3] E. A. DeWolf, I. M. Dremin, and W. Kittel, Phys. Rep. **270**, 1 (1996).
  - [4] See also the proceedings of a series of workshops that followed the Shandong Workshop [2]. Some of them are: F. Cooper, R.C. Hwa, and I. Sarcevic, *Intermittency in High energy Collisions* (World Scientific, Singapore, 1991); R.C. Hwa, W. Ochs, and N. Schmitz, *Fluctuations and Fractal Structure* (World Scientific, Singapore, 1992); R.C. Hwa, W. Kittel, W.J. Metzger, and J. Schotanus, *Correlations and Fluctuations* (World Scientific, Singapore, 1997).
  - [5] J. Dias de Deus, Nucl. Phys. **B59**, 231 (1973); A.J. Buras and J. Dias de Deus, *ibid.* **B71**, 481 (1974).
  - [6] Z. Koba, H.B. Nielsen, and P. Olesen, Nucl. Phys. **B40**, 317 (1972).
  - [7] R.C. Hwa and J.C. Pan, Phys. Rev. D **45**, 106 (1992); J.C. Pan and R.C. Hwa, Phys. Rev. D **48**, 168 (1993).
  - [8] A. Białas and R. Peschanski, Nucl. Phys. B **273**, 703 (1986); **308**, 857 (1988).
  - [9] T. Sjöstrand, Comp. Phys. Commun. **39**, 347 (1986); T. Sjöstrand and M. Bengtsson, Comp. Phys. Commun. **43**, 367 (1987).
  - [10] A. Capella, U. Sukhatme, C.I. Tan, and J. Tran Thanh Van, Phys. Lett. **81B**, 68 (1979); Phys. Rep. **236**, 225 (1994).
  - [11] R.P. Feynman, Phys. Rev. Lett. **23**, 1415 (1969).
  - [12] K.P. Das and R.C. Hwa, Phys. Lett. **68B**, 459 (1977); R.C. Hwa, Phys. Rev. D **22**, 1593 (1980).
  - [13] B. Andersson, G. Gustafson, and B. Nilsson-Almqvist, Nucl. Phys. B **281**, 289 (1987); B. Nilsson-Almqvist and E. Stenlund, Phys. Commun. **43**, 387 (1987).
  - [14] W.R. Chen and R.C. Hwa, Phys. Rev. D **36**, 760 (1987); W.R. Chen and R.C. Hwa and W.N. Wang, Phys. Rev. D **38**, 3394 (1988);
  - [15] V.V. Anisovich, M.N. Kобрinsky, J. Nyiri, and Yu.M. Shabelski, *Quark Model and High Energy Collisions* (World Scientific, Singapore, 1985).
  - [16] A.W. Chao and C.N. Yang, Phys. Rev. D **8**, 2063 (1973).
  - [17] T.T. Chou and C.N. Yang, Phys. Rev. **170**, 1591 (1968); Phys. Rev. Lett. **20**, 1213 (1968).
  - [18] R.C. Hwa and X.N. Wang, Phys. Rev. D **39**, 2561 (1989).
  - [19] A. Breakston *et al.*, Phys. Rev. D **30**, 528 (1984); G.J. Alner *et al.* (UA5 Collaboration), Phys. Lett. **160B**, 199 (1985); M. Adamus *et al.* (EHS/NA22 Collaboration), Z. Phys. **C 32**, 475 (1986); M. Adamus *et al.* (EHS/NA22 Collaboration), Z. Phys. **C 39**, 311 (1988).
  - [20] Aguilar-Benitez *et al.* (LEBC-EHS Collaboration), Z. Phys. **C 50**, 405 (1991).
  - [21] W. Thome *et al.*, Nucl. Phys. **B129**, 365 (1977).
  - [22] M. Adamus *et al.* (EHS/NA22 Collaboration), Z. Phys. **C 37**, 215 (1988).
  - [23] W.R. Chen and R.C. Hwa, Phys. Rev. D **39**, 179 (1989).
  - [24] X.N. Wang, Phys. Rev. D **43**, 104 (1991).
  - [25] I.V. Ajineko *et al.* (NA 22), Phys. Lett. B **222**, 306 (1989); **235**, 373 (1990).
  - [26] C. Albajar *et al.* (UA1), Nucl. Phys. B **345**, 1 (1990); N. Neumeister *et al.*, Z. Phys. **C 60**, 633 (1993).
  - [27] N. M. Agababyan *et al.* (NA 22), Z. Phys. **C 59**, 405 (1993).

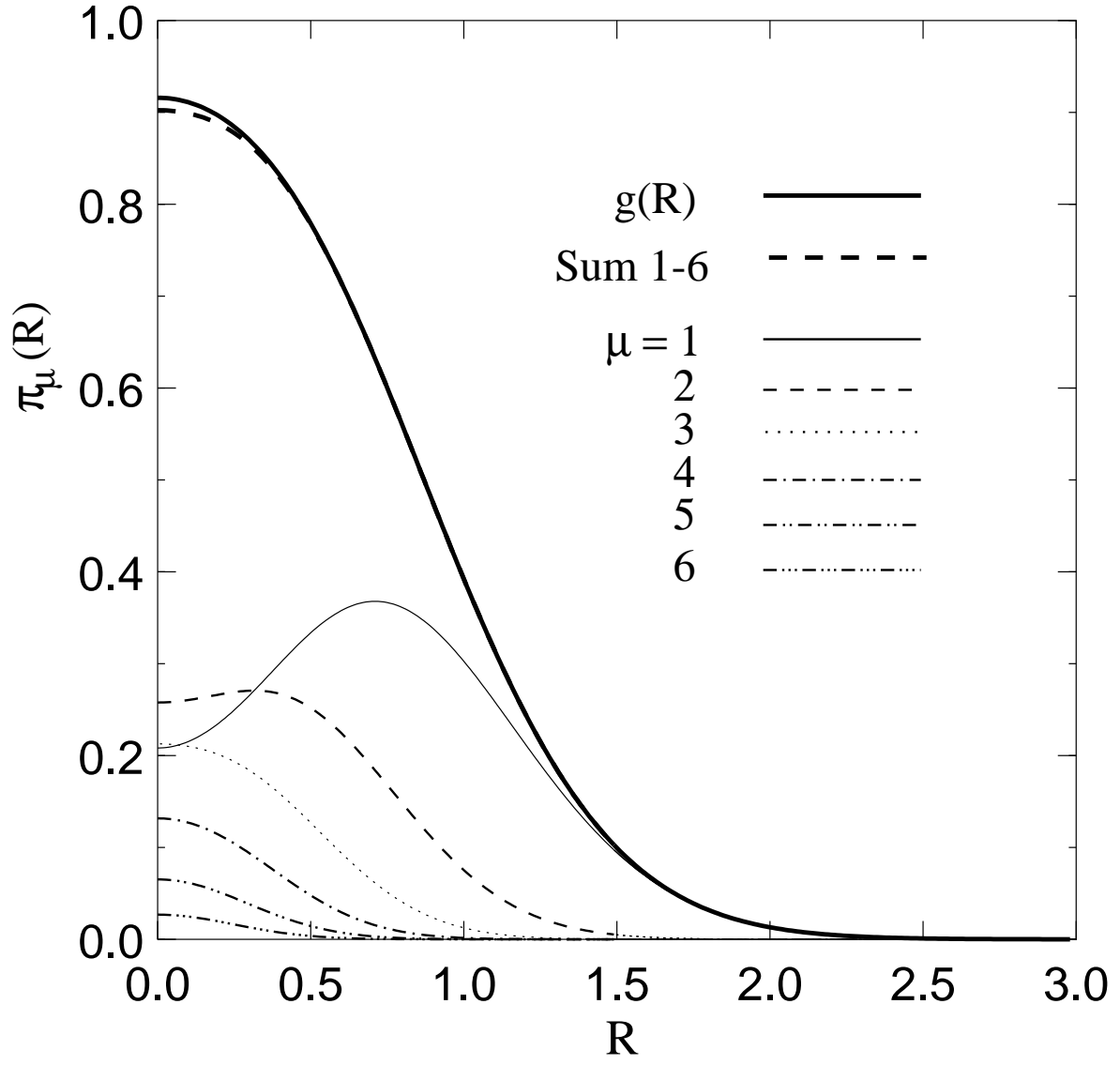


FIG. 1. Probability of having  $\mu$ -cut Pomerons at  $R$ .



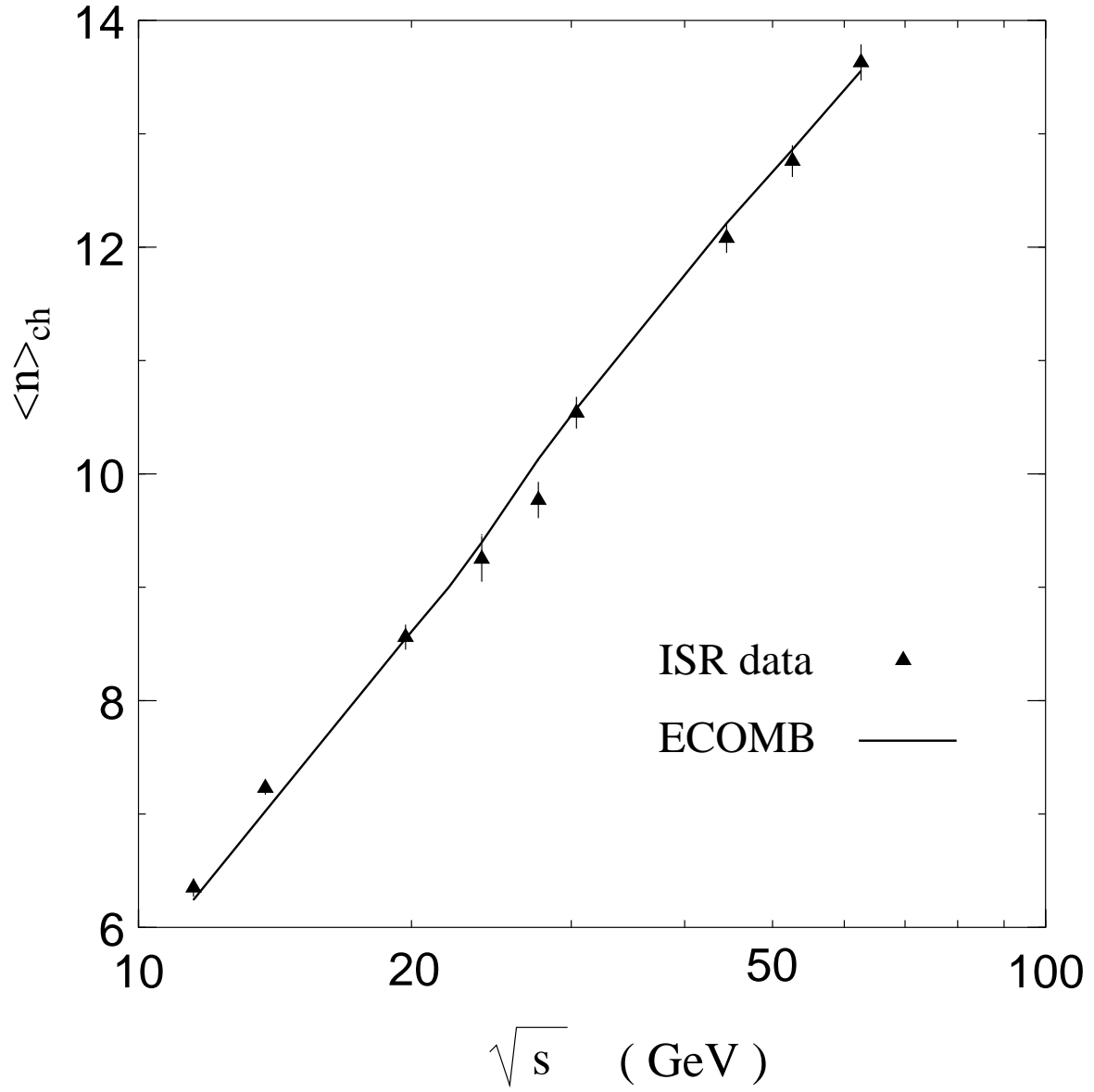


FIG. 2. Average charge multiplicity as a function of cm energy. The data are from [19].

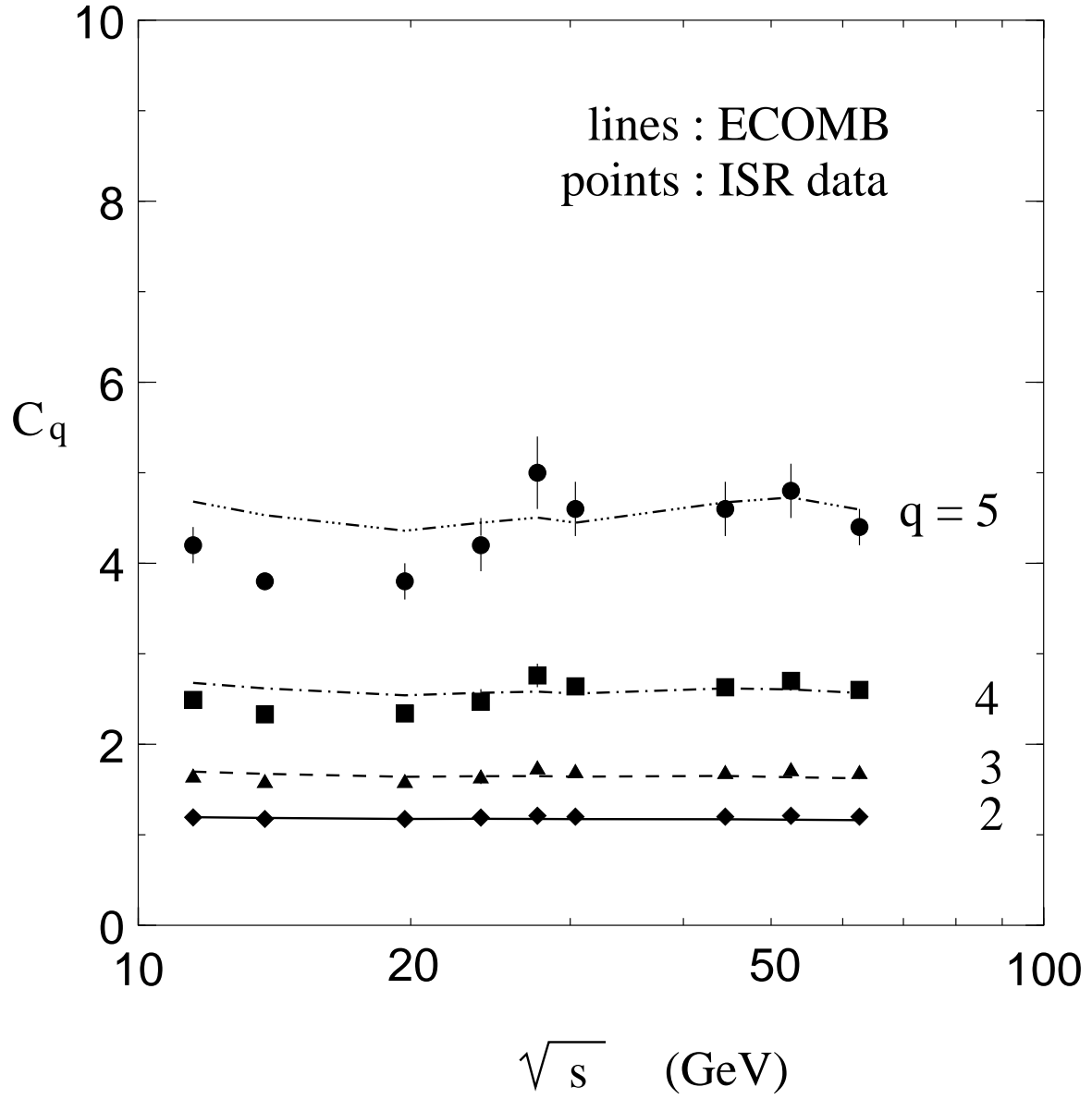


FIG. 3. Standard moments of the multiplicity distribution. The data are from [19].

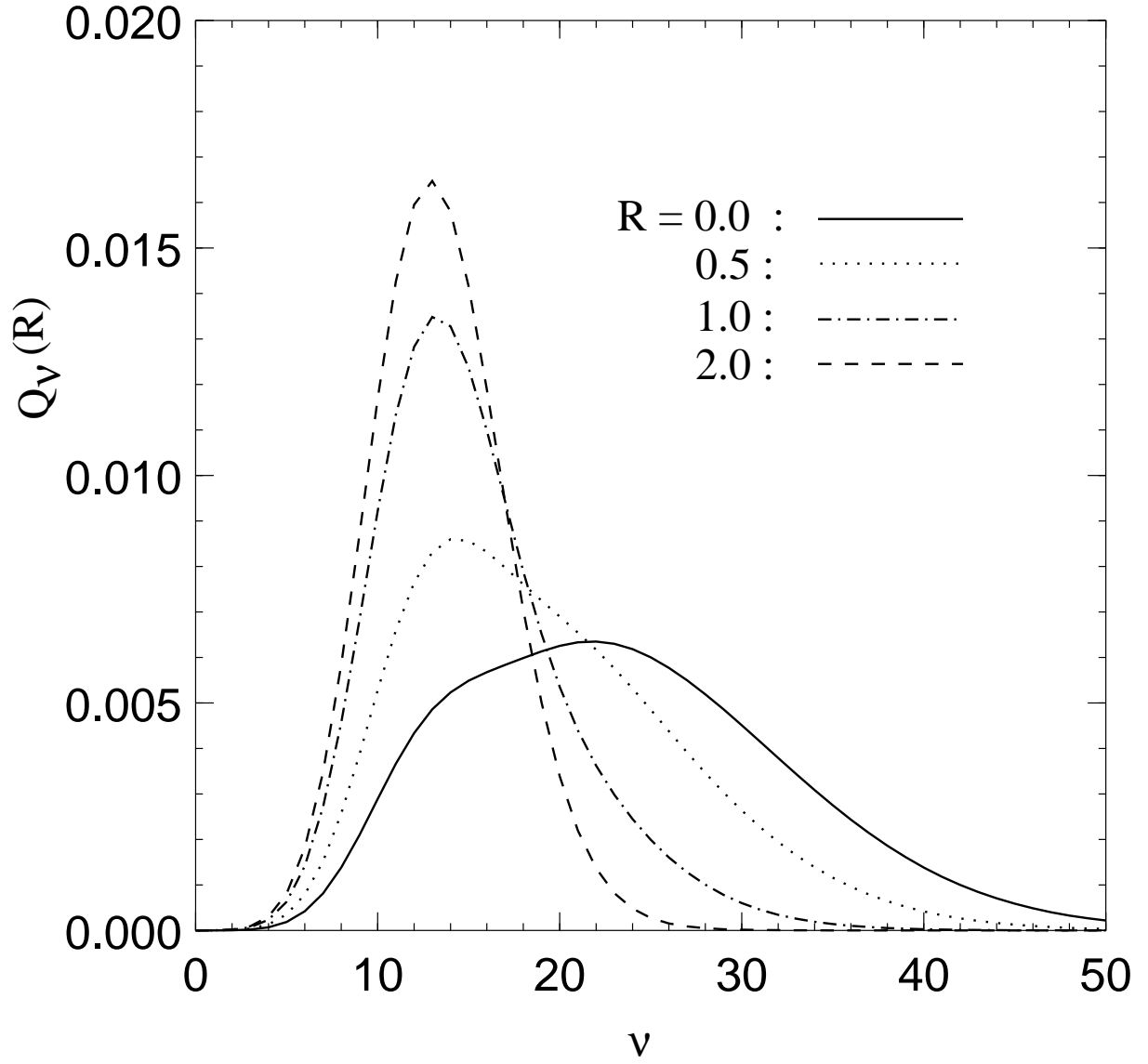


FIG. 4. The distributions of parton numbers at various fixed  $R$ .

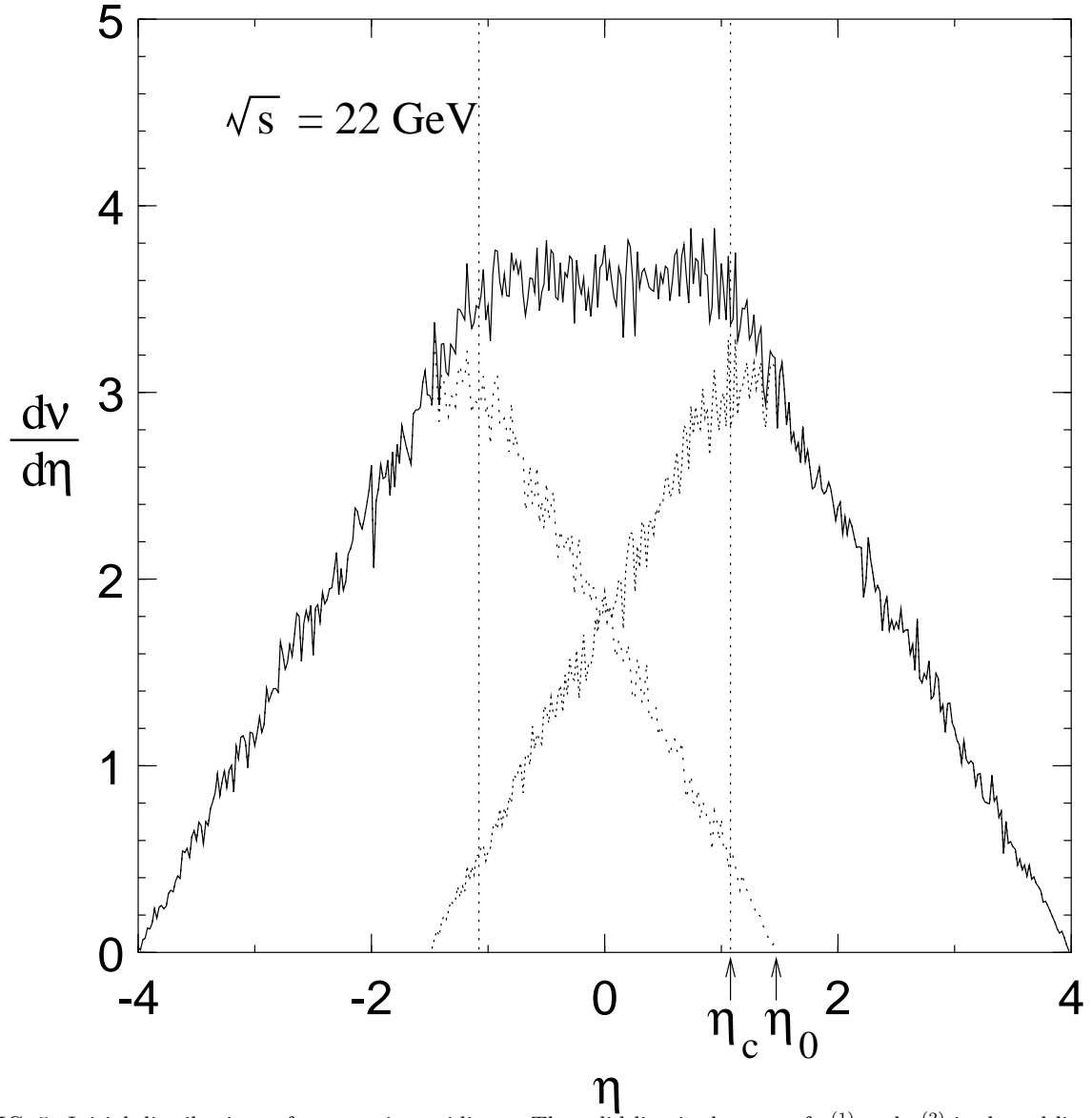
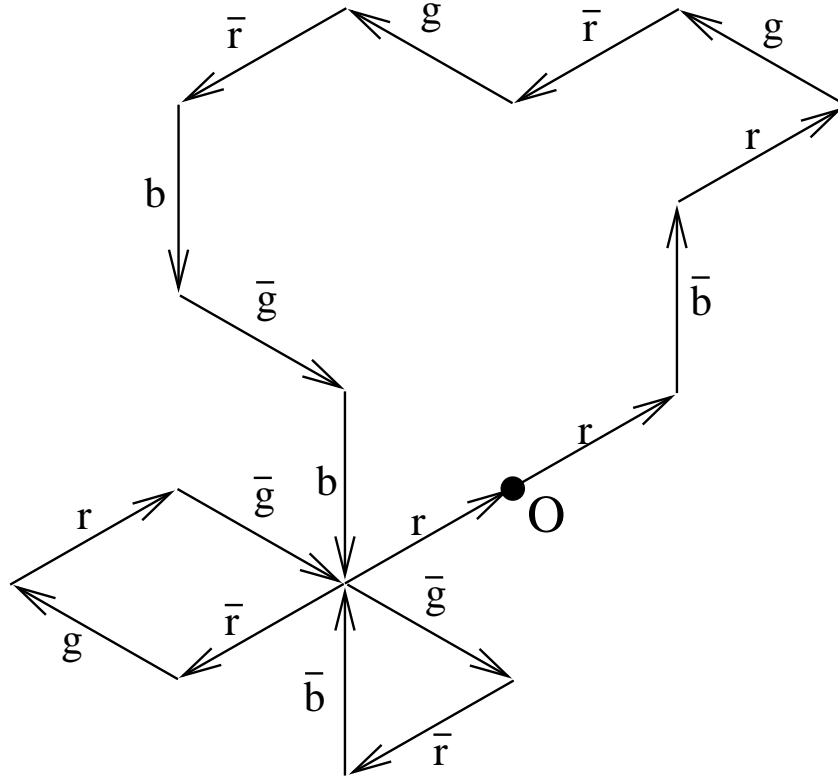


FIG. 5. Initial distributions of partons in rapidity  $\eta$ . The solid line is the sum of  $\rho^{(1)}$  and  $\rho^{(2)}$  in dotted lines.



$$r \bar{b} r g \bar{r} g \bar{r} b \bar{g} b \bar{r} g r \bar{g} \bar{g} \bar{r} \bar{b} r$$

FIG. 6. A sample path in color space for a configuration of partons arranged in the array shown.

# of partons : 24

B : Blue

G : Green

R : Red

b : Anti-blue

g : Anti-green

r : Anti-red

1	BGGBgbBgGggbbbgGGRBBGrb														
2	BGGgBBgGggbbbgGGRBBGbr														
3	GGBgBBgggbGbbbgGgGBRGbrB														
4	GBgBGgBgbGgbbgbGgBRGGbBr														
5	GBgBgBGbggbbGbGggBRGbGBr														
6	BGggBGbBgbbGgbggBRGbGBrG														
<div></div>															
7	GBgBgbBGgbGb							gbggRBGGbBGr							
8	BgBgbBGgGGbb							ggbgRGBbGGrB							
9	gBgbBBGgGbGb							gbggRGBGbrGB							
10	BgbBBggGbGGB							gggbGRGbrGBB							
11	BgbBBgGbgGGB							gggbRGGbGBBr							
12	BbBBggGbGGB							ggbgGRGbBBrG							
<div></div>															
13	bB	BBgGbggGbG					gbgGgGRbBrGB								
14	bB	BBGbgggGGb					bggGGRgBrGBb								
<div></div>															
15	Bb	BGbgBggGbG					bgGGggRrGB					bB			
<div></div>															
16	Bb	BbGg		gBGbgG			gbGGggrGBR					Bb			
<div></div>															
17	bB	Bb	gG	BGgb	Gg	gbGGgrgGBR					bB				
18	Bb	bB	Gg	GBgb	gG	gbGgGrgBGR					bB				
19	bB	bB	Gg	BGgb	gG	gGgbGgrBRG					Bb				
<div></div>															
20	bB	bB	gG	GBbg	gG	Gg	gGgrBRGb				Bb				
<div></div>															
21	Bb	bB	Gg	GbBg	gG	gG	gG	grBRGb				bB			
22	Bb	Bb	gG	GBgb	Gg	Gg	Gg	rBgGbR				bB			
23	bB	bB	gG	BGgb	gG	Gg	Gg	BrgbGR				bB			
24	Bb	Bb	Gg	BGgb	gG	gG	gG	rgBbRG				bB			
25	Bb	Bb	Gg	GBbg	Gg	Gg	Gg	rgbBRG				Bb			
26	Bb	bB	gG	GBbg	Gg	Gg	Gg	rbgBGR				Bb			
27	Bb	Bb	gG	BGgb	gG	gG	gG	brBgRG				bB			
28	Bb	bB	Gg	GbBg	gG	gG	gG	brBgRG				Bb			
29	Bb	bB	gG	GBgb	gG	Gg	gG	rbBgRG				bB			
30	Bb	Bb	gG	BgbG	Gg	Gg	gG	rBbRgG				Bb			
<div></div>															
31	bB	Bb	gG	BbgG	gG	Gg	gG	BbRr		Gg	Bb				
<div></div>															
32	bB	Bb	gG	Bb	gG	gG	Gg	gG	Bb	Rr	Gg	Bb			

FIG. 7. An example of a branching process that starts with 24 partons. The numbers in the first column denote the number of time steps taken for the configuration in any particular row.

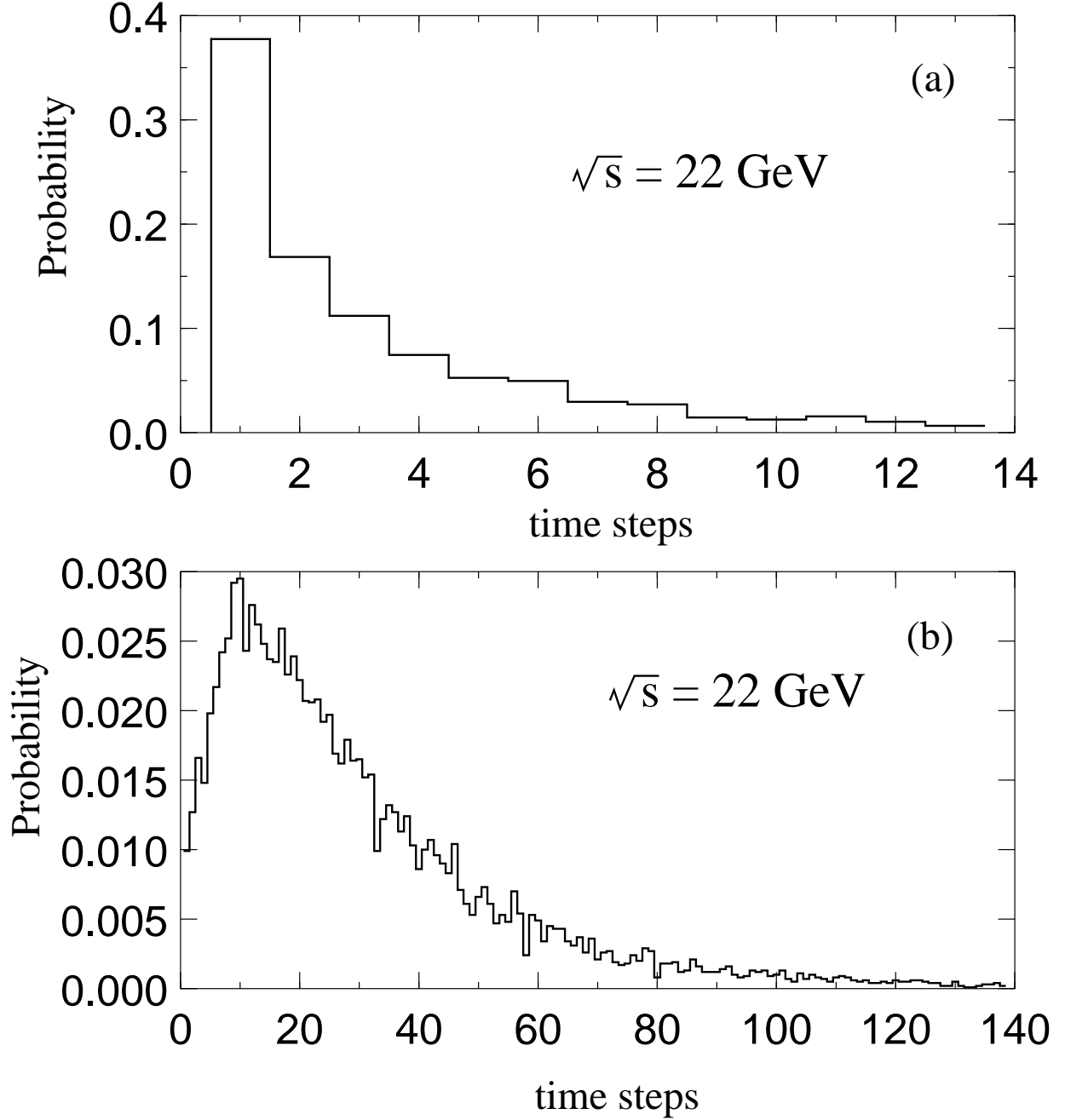


FIG. 8. (a) The distribution of times steps taken for 20 initial partons before a fission process occurs. (b) The distribution of time steps taken for the 20 partons to evolve to the end when branching terminates.

$$E = 22 \quad 23.6 \quad 30.8 \quad 45.2 \quad 53.2 \quad 63.2 \text{ GeV}$$

○ ◇ ◆ ▲ ■ ●

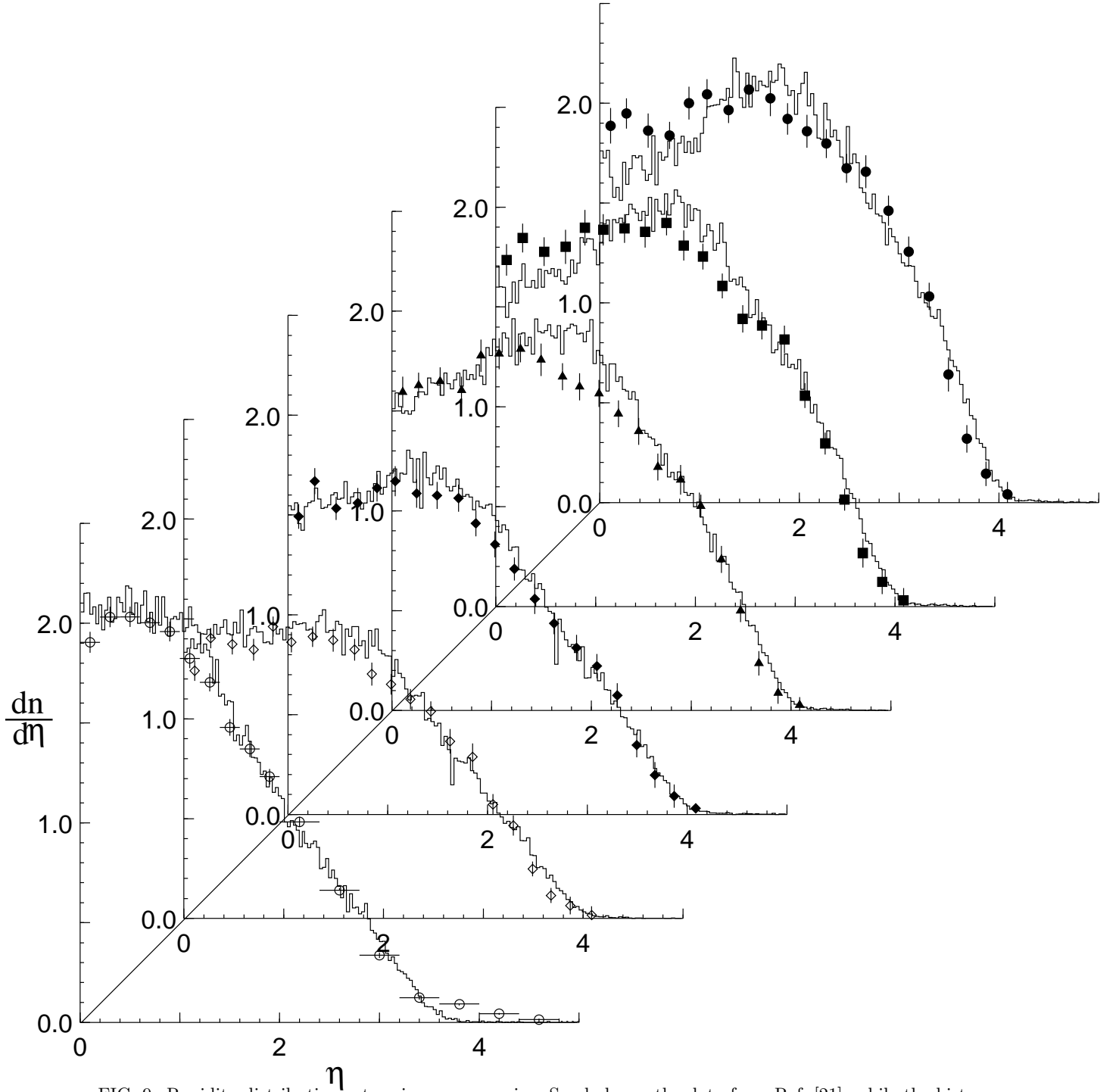


FIG. 9. Rapidity distributions at various cm energies. Symbols are the data from Ref. [21], while the histograms are the result of ECOMB.



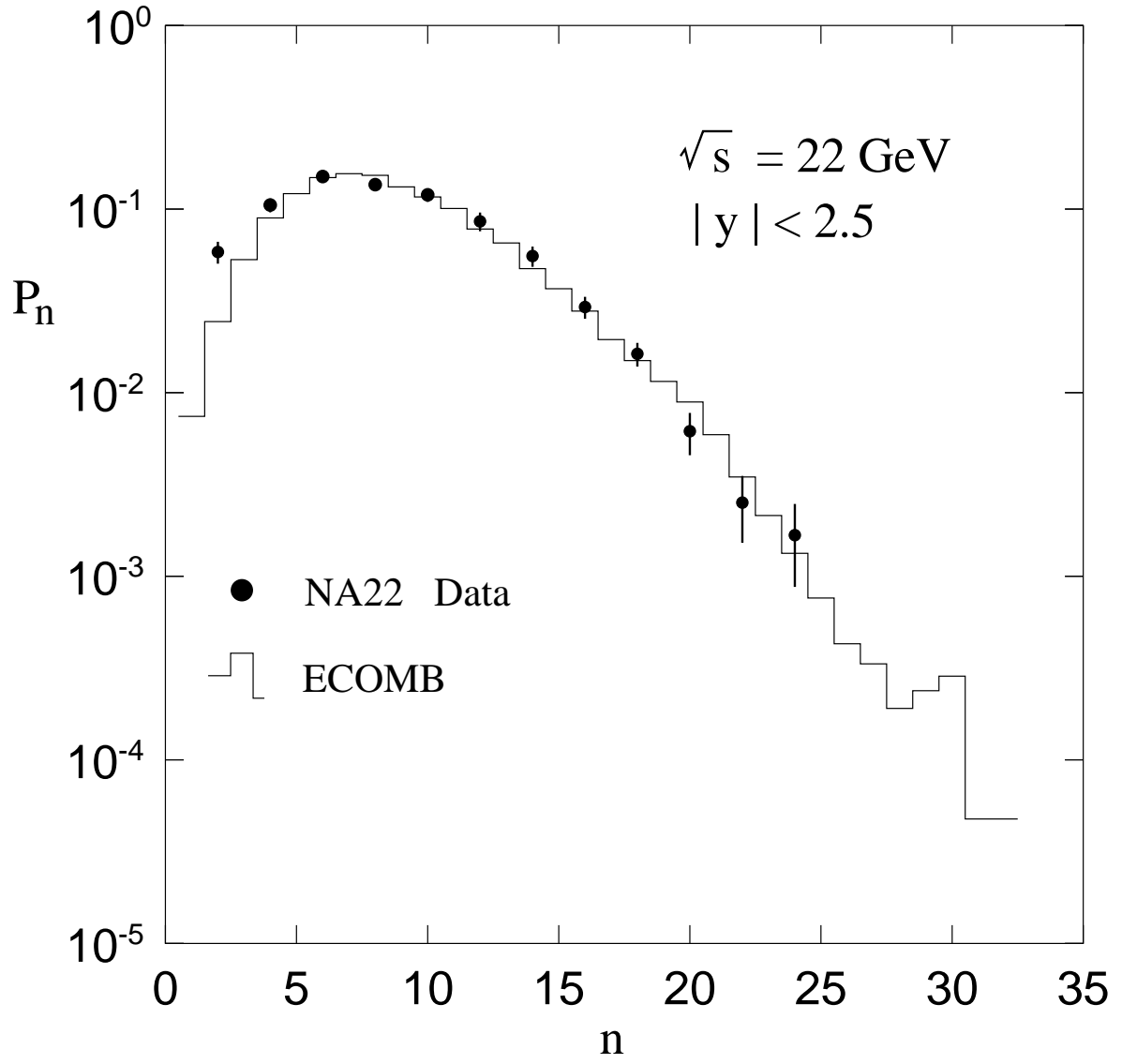


FIG. 10. Multiplicity distributions of charged particles. The data are from Ref. [22].

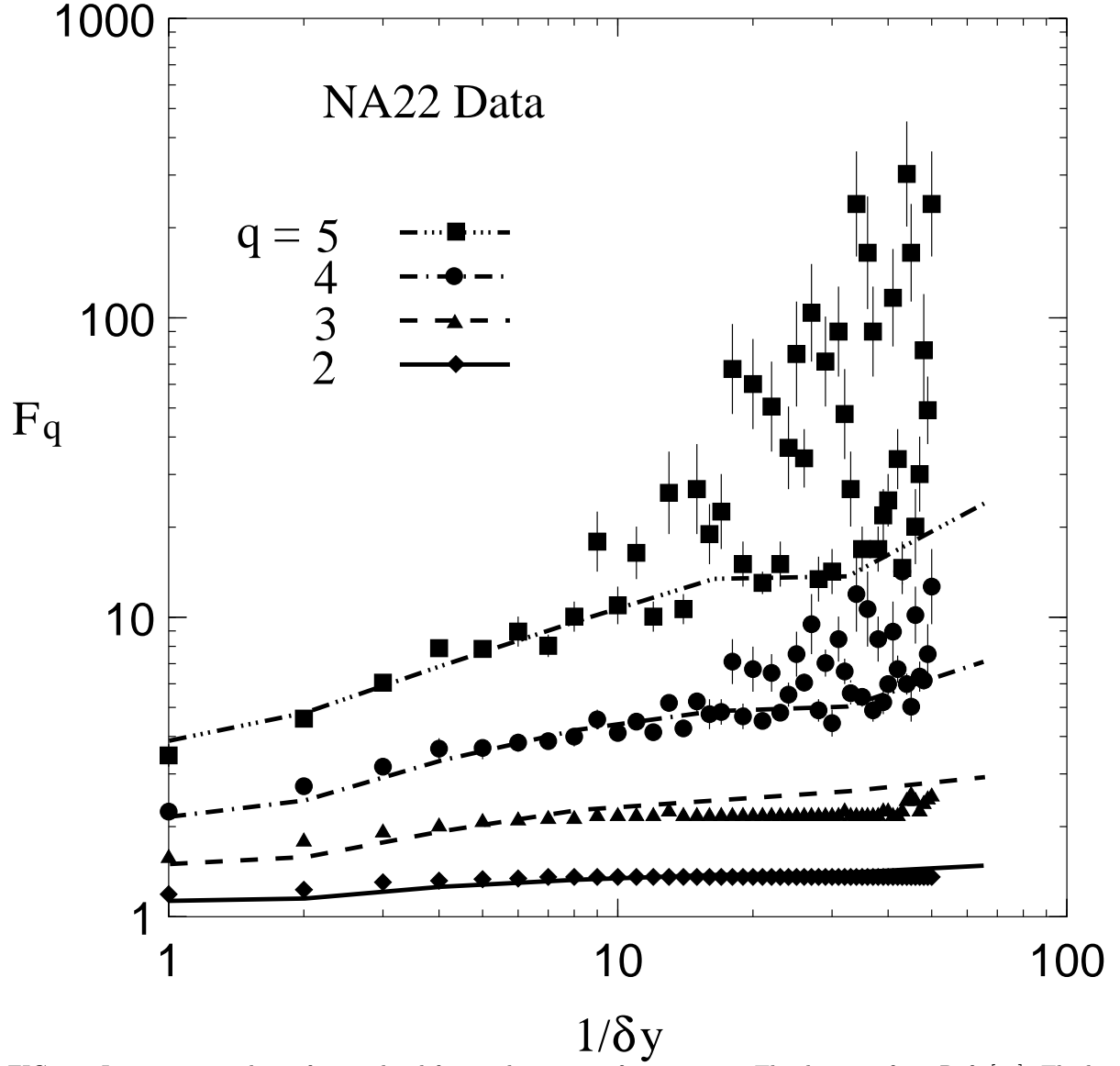


FIG. 11. Intermittency data of normalized factorial moments for  $q = 2 - 5$ . The data are from Ref. [25]. The lines are determined from ECOMB.